Earth and Planetary Science Letters 468 (2017) 94–100

Contents lists available at ScienceDirect

Earth and Planetary Science Letters

www.elsevier.com/locate/epsl

The finite, kinematic rupture properties of great-sized earthquakes since 1990

Gavin P. Hayes

U.S. Geological Survey National Earthquake Information Center, United States

ARTICLE INFO

Article history:
Received 10 February 2017
Received in revised form 31 March 2017
Accepted 1 April 2017
Available online 19 April 2017
Editor: P. Shearer

Keywords:
finite fault modeling
source inversion
earthquake potency
great earthquakes
earthquake cycles

ABSTRACT

Here, I present a database of >160 finite fault models for all earthquakes of M 7.5 and above since 1990, created using a consistent modeling approach. The use of a common approach facilitates easier comparisons between models, and reduces uncertainties that arise when comparing models generated by different authors, data sets and modeling techniques.

I use this database to verify published scaling relationships, and for the first time show a clear and intriguing relationship between maximum potency (the product of slip and area) and average potency for a given earthquake. This relationship implies that earthquakes do not reach the potential size given by the tectonic load of a fault (sometimes called "moment deficit," calculated via a plate rate over time since the last earthquake, multiplied by geodetic fault coupling). Instead, average potency (or slip) scales with but is less than maximum potency (dictated by tectonic loading). Importantly, this relationship facilitates a more accurate assessment of maximum earthquake size for a given fault segment, and thus has implications for long-term hazard assessments. The relationship also suggests earthquake cycles may not completely reset after a large earthquake, and thus repeat rates of such events may appear shorter than is expected from tectonic loading. This in turn may help explain the phenomenon of "earthquake super-cycles" observed in some global subduction zones.

Published by Elsevier B.V.

1. Introduction

In modern global seismology, a key step in the analysis of source properties of a large earthquake is the construction of a finite fault model, used to constrain the slip distribution of the earthquake on its fault plane in either a static (if using non-continuous geodetic data) or kinematic (using seismic, continuous GPS or tsunami data) sense. Since the first applications of finite fault inversion approaches in the 1970s and 80s (e.g., Alewine, 1974; Langston, 1978; Heaton and Helmberger, 1979; Hartzell and Helmberger, 1982; Hartzell and Heaton, 1983), and the expansion of the field since the 1990s associated with the availability of digital broadband seismic data (e.g., Kikuchi and Kanamori, 1991; Ji et al., 2002), a variety of approaches and data sets have been used to explore source finiteness; for a review, see Ide (2007).

Today, numerous models that describe the rupture history of a recent large earthquake are publicly available soon after the event. For example, recent earthquake pages of the U.S. Geological Survey (USGS) National Earthquake Information Center (NEIC) routinely provide finite fault models for large global earthquakes. Other academic institutions (e.g., University of California Santa Cruz, http://www.geol.ucsb.edu/faculty/ji/; University of Tsukuba, http://www.geol.tsukuba.ac.jp/~yagi-y/eng/earthquakes.html; Caltech Tectonics Observatory, http://www.tectonics.caltech.edu/slip_history/index.html) provide similar models on a case-by-case basis. Peer reviewed literature also contains detailed descriptions of major earthquakes (e.g., for the 2011 M9.0 Tohoku earthquake, Ammon et al., 2011; Hayes, 2011; Hayes et al., 2011; Ide et al., 2011; Koketsu et al., 2011; Lay et al., 2011; Ozawa et al., 2011; Pollitz et al., 2011; Shao et al., 2011; Simons et al., 2011; Yagi and Fukahata, 2011; Yue and Lay, 2011; Wei et al., 2012).

Despite the abundance of rupture models for recent events, few databases exist that catalog models and facilitate the comparison of one model to another, or one event to another. There are two notable exceptions. The first is the excellent Finite-Source Rupture Model Database known as SRCMOD (Mai and Thingbaijam, 2014). This compilation includes over 330 models for close to 170 earthquakes (as of June 2016), and is an excellent source for researchers wishing to explore the nature of earthquake rupture. Mai and Thingbaijam (2014) provide an overview of the various uses of such model suites.

While the SRCMOD database does include multiple models from several authors, and a broad range of models for different

E-mail address: ghayes@usgs.gov.

http://dx.doi.org/10.1016/j.epsl.2017.04.003
0012-821X/Published by Elsevier B.V.

events, it does not provide a comprehensive analysis of all large earthquakes over a given time period, analyzed using a consistent approach and unified framework. As a result, any study using such models to analyze, for example, the source scaling of earthquakes (e.g., Mai and Beroza, 2000; Blaser et al., 2010, and references therein) will be sensitive to uncertainties arising from differences in modeling techniques and parameterization (e.g., Thingbaijam and Mai, 2016), in addition to those inherent in any individual modeling approach. These uncertainties can be reduced, to a certain extent, by comparing only those models that have been generated using a consistent modeling approach—this goal is something I attempt to address here.

This is also attempted by Ye et al. (2016), who produce a database of finite fault models for $M \geq 7.0$ subduction interface earthquakes following a consistent approach, albeit only for megathrust earthquakes. Their compilation of over 100 finite fault models (available at https://sites.google.com/site/linglingye001/earthquakes/slip-models) is an excellent complement to this study. I attempt to broaden the Ye et al. database further by also considering non-subduction related earthquakes over the same time period.

To that end, I describe and provide a finite fault database for all shallow (0–70 km) and intermediate-depth (70–300 km), $M \geq 7.5$ earthquakes since 1990 (Fig. 1, Table S1), all modeled using the same inversion procedure (Ji et al., 2002). For all earthquakes in the database, I have undertaken a comprehensive analysis of their rupture history using broadband teleseismic data; testing sensitivity to key uncertainties like fault geometry, rupture velocity and hypocentral depth, and using other constraints where available (e.g., published studies or fault geometry databases like the USGS Slab1.0 model, Hayes et al., 2012) to derive a single best-fitting model for each event. The 2004 M 9.2 Sumatra earthquake is excluded from this dataset due to the difficulty in modeling this long-duration event with teleseismic data alone.

The database has been published online through the USGS NEIC Combined Catalog (ComCat, http://earthquake.usgs.gov/earthquakes/map/), and can be viewed there on individual event pages and through the broader earthquake search engine (http://earthquake.usgs.gov/earthquakes/search/). For each model, a series of downloadable files are included that describe: (i) the finite fault itself (in both a static format familiar to users of rapid NEIC fault models, and in the new SRCMOD Finite Source Parameter (FSP) format, Mai et al., 2016); (ii) an ASCII source time function for the event; (iii) the global Centroid Moment Tensor (gCMT) CMTSOLUTION for each sub-event (http://globalcmt.org); (iv) input files for the Coulomb3 software package (Toda et al., 2005, 2011 and (v) three-components of predicted ground deformation, computed using the Okada (1992) formulation on a grid surrounding the surface expression of the model. The FSP formatted files, providing a comprehensive description of each model, have also been uploaded to the SRCMOD database. Each file is described in more detail in the Supplementary Materials. The modeling approach followed here is the same as is used for all recent earthquakes of $M >\sim 7.0$ at the USGS NEIC, ensuring the continuation of the database into the future.

2. Modeling approach

The database employs a finite fault inversion approach based on the method of Ji et al. (2002), used often in USGS studies (e.g., Table 1). The procedure inverts both body-wave (P and SH, band-pass filtered between 1 and 200 s) and surface wave (Rayleigh and Love, band-pass filtered between 200 and 500 s) data on a fault surface defined *a priori*, typically aligned with estimates from CMT (either USGS W-phase or gCMT) solutions. Both nodal planes of the initial CMT solution are tested to account for the uncertainty over which plane describes the causative fault, and may further divide a favored plane into multiple fault segments if required by the data or suggested by other information. Similarly, strike and dip of the inverted fault plane (or planes) are systematically varied from the initial geometry to test model sensitivity to these assumptions.

Data are chosen based on producing an azimuthally balanced data set, while avoiding the inclusion of data with small signal-to-noise ratios. Rupture velocity can be fixed or allowed to vary; to account for unknown rupture characteristics, variable velocities are tested, as are a broad distribution of fixed velocities, before settling on a final model where rupture velocity is allowed to vary about a favored fixed value. Initial fault length is estimated from empirical relations between duration and moment (Dahlen and Tromp, 1998), scaled to length assuming a rupture velocity of 2.5 km/s, and doubled to account for uncertainty in rupture direction (i.e., centered bilaterally on the hypocenter).

Fault planes are divided into a series of sub-faults along the strike and dip directions, and the inversion solves for the slip amplitude, slip direction, rise-time and rupture initiation time of each sub-fault, where sub-fault source time functions are modeled with an asymmetric cosine function (Ji et al., 2002, 2003). The model is referenced spatially to the USGS NEIC hypocenter, at least initially; as with other key parameters, location is varied when other information (e.g., regional network solutions and/or published studies) indicates a necessary relocation.

Using this approach, several models in the database have been previously published in peer reviewed literature, as indicated in Table 1. In Section 3, I discuss how the entire collection of models might be used, and how they can be and are being used by others to advance our understanding of the earthquake source.

Table 1
Models in the database that have been published and peer reviewed.

Event name	Date	Magnitude (Mw)	Reference
Puysegur	2009-07-15	7.8	Hayes and Furlong (2010)
Maule	2010-02-27	8.8	Hayes et al. (2013)
Mentawai	2010-10-25	7.8	Newman et al. (2011)
Tohoku	2011-03-11	9.0	Hayes (2011) Hayes et al. (2011) Wei et al. (2014)
Santa Cruz Islands	2013-02-06	8.0	Hayes et al. (2014a)
Iquique	2014-04-01	8.2	Hayes et al. (2014b)
	2014-04-03	7.7	
Nepal	2015-04-25	7.8	Hayes et al. (2015)

3. Database uses

Many of the studies listed in Table 1 focus on the use of finite fault models for seismotectonic characterizations of major earthquake sequences, like Tohoku (Hayes, 2011), Maule (Hayes et al., 2013), the Santa Cruz Islands (Hayes et al., 2014a), Iquique (Hayes et al., 2014b), and Nepal (Hayes et al., 2015). In these studies, the mainshock slip distribution is combined with detection and relocation efforts for fore- and aftershocks, improving catalog completeness, minimally biased earthquake locations with accurate uncertainties, and with moment tensor analyses of the same events, to provide a comprehensive analysis of the spatiotemporal evolution of the sequence, how it relates to the history of seismicity and tectonics in the region, and how it may be interpreted within the framework of subduction zone seismogenesis (where appropriate). Such analyses are becoming routine at the NEIC after the occurrence of a major earthquake, in the hope that these studies will ultimately facilitate broader comparisons of sequences within an individual subduction zone (e.g., Maule vs. Iquique, Hayes et al., 2014b) or other tectonic environment, and between different margins around the world.

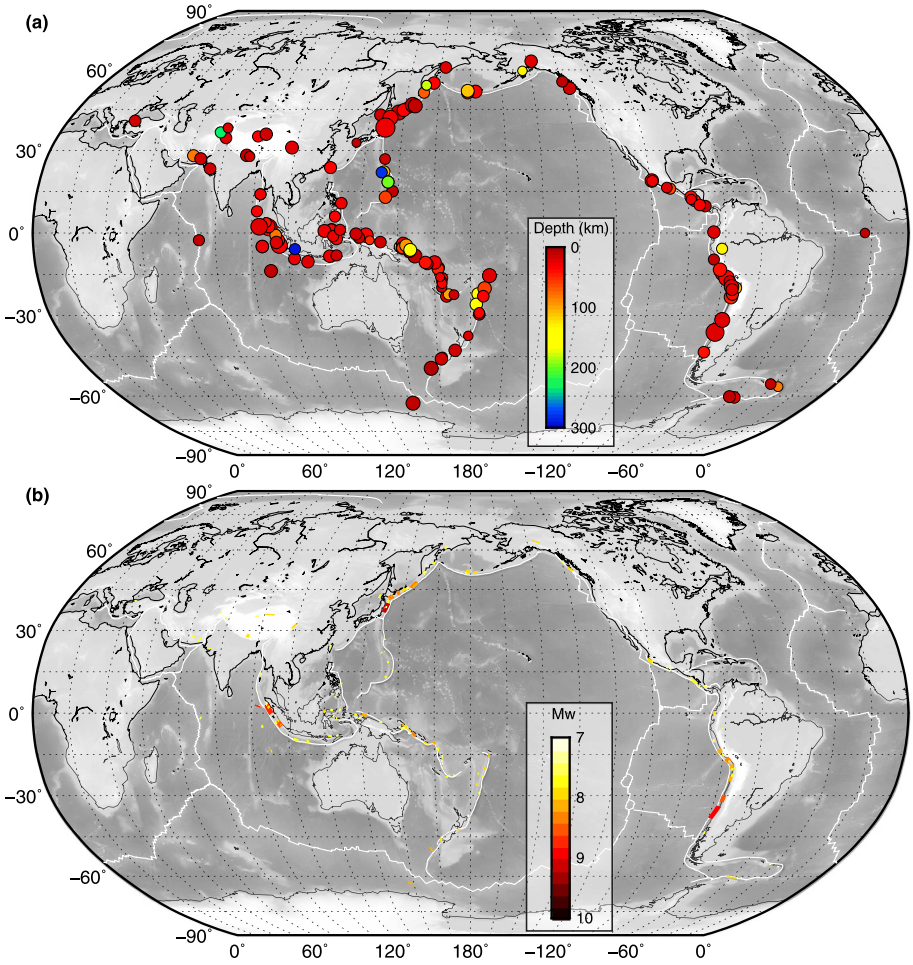

Fig. 1. Global distribution of earthquakes for which finite fault models are presented as part of this database. In (a), earthquake hypocenters are sized by magnitude and colored by their depth. In (b), the approximate source dimensions of each event, as computed using the autocorrelation function of Mai and Beroza (2000), are plotted. Rectangles of each rupture surface are colored by the moment magnitude of the event.

Tsunami models are another popular use of finite fault solutions, as demonstrated by a variety of publications that have used models from our database (e.g., Hayes and Furlong, 2010; Okal et al., 2010; Roeber et al., 2010; Newman et al., 2011; Fritz et al., 2011; Wei et al., 2014; Riquelme et al., 2015). Finite fault models produced at the NEIC via the inversion of teleseismic data have proven particularly useful for tsunami modeling because they are generally available within hours of the occurrence of a major earthquake (e.g., Hayes et al., 2011), and thus have important applications for real-time monitoring (e.g., Wang et al., 2012).

Finite fault models from our database can also be readily used to study the surface deformation generated by an earthquake, an effort made easier with this database update through the provision of an Okada-based (Okada, 1992) deformation field in the *Downloads* section of each model page (*.disp* files, Supplementary Material). Such comparisons have proven useful in the past as a way of assessing the accuracy of a suite of different models (e.g., Vigny et al., 2011; Hayes et al., 2013), and in combination with earthquake relocation studies to iteratively improve teleseismic based finite-fault models and their forward predictions of surface deformation data (e.g., Barnhart et al., 2014a, 2014b).

Finally, as previously mentioned, this database provides a means by which to create source scaling relationships for large earthquakes (e.g., Wells and Coppersmith, 1994; Mai and Beroza, 2000; Blaser et al., 2010; Skarlatoudis et al., 2016) using models generated via a consistent approach, rather than being vulnerable to uncertainties arising through the comparisons of models produced with differing assumptions. Similarly, models can be combined with fault databases like Slab1.0 (Hayes et al., 2012) to derive scaling relationships for use in rapid ground-shaking and impact assessments (Allen and Hayes, 2017), vital for post-earthquake rapid response efforts at the NEIC (e.g., Wald et al., 2005, 2008).

4. Scaling implications

Here, I briefly analyze what these models can tell us about source scaling, a topic of broad interest with obvious applications for seismic hazard analyses (e.g., Petersen et al., 2014). First, because initial fault dimensions are set somewhat arbitrarily—to be larger than the true source dimensions such that slip naturally tapers to zero at the edge of each model (in an ideal scenario)—models must be trimmed to estimate 'true' source dimensions. I follow the approach of Mai and Beroza (2000), who use an autocorrelation of the slip distribution to approximate slip length and width (Fig. 2, Table S1). In Allen and Hayes (2017), we use an alternate approach that compares sub-fault moment to peak moment to trim the fault and derive fault dimensions. There, we also discuss the uncertainties on those dimensions and how estimates compare following the two different approaches; I refer readers to that study for further details.

Fig. 3 compares the relationships between moment and key source parameters like rupture length, width, and area, with

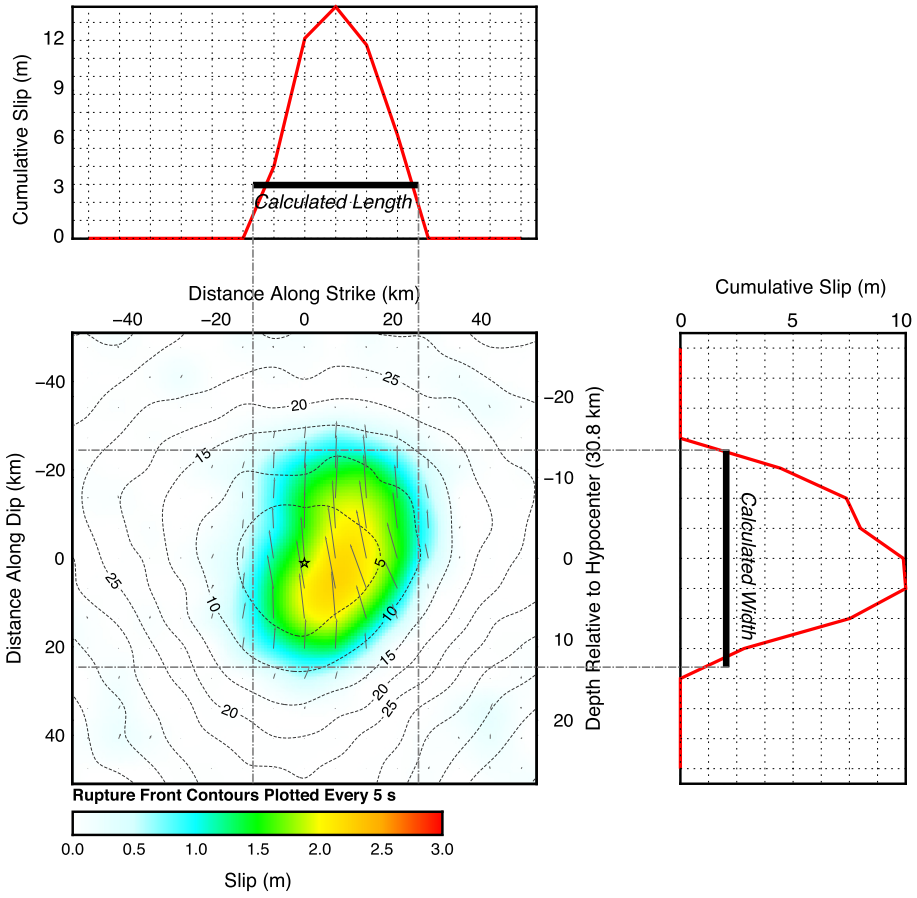

Fig. 2. Example of the calculation of fault length and width from a finite fault model using the autocorrelation function of Mai and Beroza (2000). In the main panel, fault slip is colored, and arrows represent the slip direction (rake). Contours represent the approximate location of the rupture front at the displayed time. In adjacent panels, slip is summed along strike (top) and along dip (right). Each function is then used to calculate the representative rupture length and width, displayed as black bars on each panel.

the scaling predicted by common empirical relations (Wells and Coppersmith, 1994; Mai and Beroza, 2000; Blaser et al., 2010; Skarlatoudis et al., 2016). I specifically do not derive further scaling relationships here; that work is carried out using these data in Allen and Hayes (2017). While significant scatter is evident in these comparisons, existing scaling relations predict rupture length fairly well, though both Wells and Coppersmith (1994) and Blaser et al. (2010) over-predict the length of normal and reverse faulting ruptures at lower magnitudes ($M \sim< 7.5$). Mai and Beroza (2000) chose to use one relationship for all dip slip events, which match these data very well. The Skarlatoudis et al. (2016) study provides a useful comparison to rupture width estimates because it employs width saturation, whereby rupture width is capped at some threshold related to the seismogenic width of a fault. In this sense, it is a physically reasonable model, though the width relation itself seems to over-predict estimates of rupture width reported here. The Wells and Coppersmith (1994) and Blaser et al. (2010) relations predict rupture width quite poorly for large magnitudes ($M \sim> 7.5$), though again the Mai and Beroza (2000) dip-slip relation describes these data well. As a result, the data here indicate that rupture area is best predicted by the scaling relations of Mai and Beroza (2000). It is important to note that the Wells and Coppersmith (1994) and Blaser et al. (2010) studies predominantly used rupture dimensions derived from aftershock studies, rather than from source inversions, as used in Mai and Beroza (2000) and Skarlatoudis et al. (2016). This difference may account for the fact that Mai and Beroza (2000) match data presented here better, since aftershocks typically occur on the fringes of earthquake rupture, and thus aftershock dimensions typically over-predict the true rupture dimensions of an earthquake (e.g., Mendoza and Hartzell, 1988).

Finite-fault models from different studies are often compared using peak slip. However, model sub-fault size varies from author-to-author and study-to-study, and because of this, peak slip estimates can be artificially variable. A more directly comparable quality is potency—the product of slip and area. Fig. 4 illustrates how modeled maximum potency scales with average potency, and reveals a clear linear relationship between the two. Models in the SRCMOD database (Mai and Thingbaijam, 2014) follow a similar relationship.

Correlations are also evident between maximum slip and average slip, and maximum potency and earthquake magnitude (or the logarithm of earthquake moment), in Fig. S1. These relationships show no obvious dependence on location or faulting geometry. This makes sense; excepting limited and uncertain observations of dynamic overshoot (e.g., Venkataraman and Kanamori, 2004), a coupled fault is unlikely to slip beyond its capacity to do so, dictated by tectonic loading, regardless of faulting environment. However, slip on the ruptured segment of a fault is not uniform; average potency (slip) scales with and is a fraction of maximum potency (slip). Using this constant ratio between maximum potency and average potency (or maximum slip and average slip, or maximum potency and magnitude), we can more accurately characterize how big of an earthquake can occur on a given fault segment (if the time since the last earthquake is known). We typically do this by assuming the entire area in question can slip the maximum amount given by the tectonic loading—these observations suggest that a more accurate estimate can be provided using the relationship between maximum potency (slip) and average potency

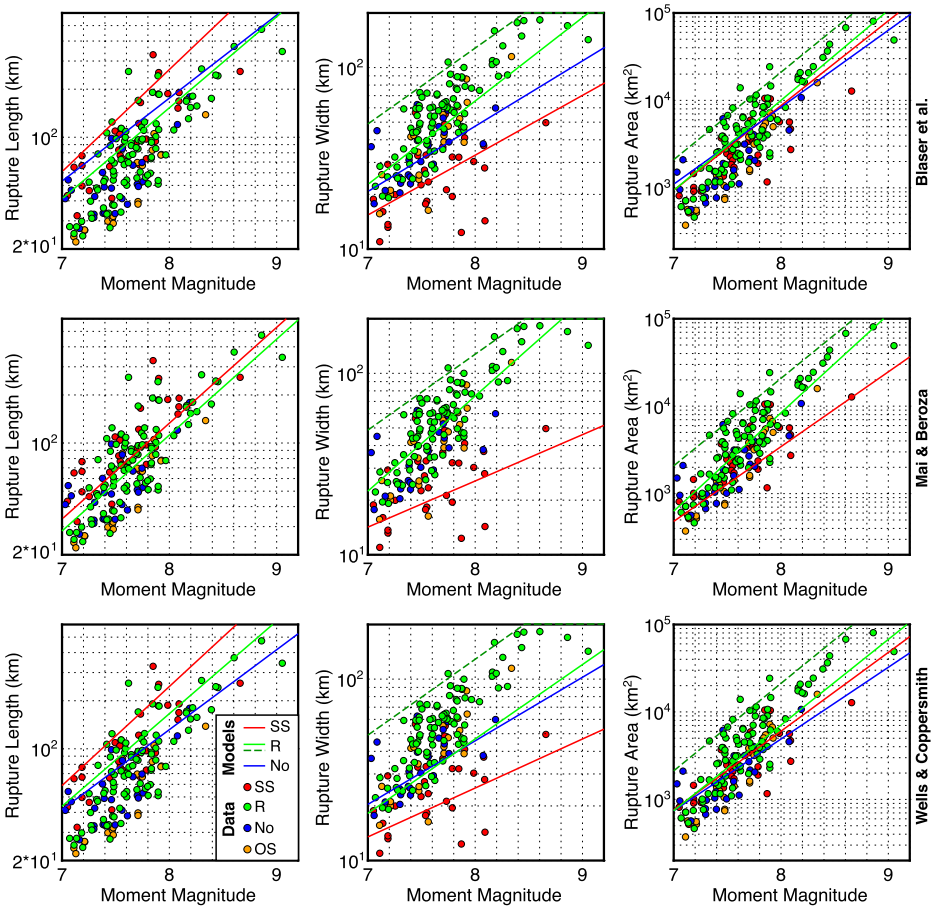

Fig. 3. Relationship between earthquake moment magnitude and, respectively, from left to right: rupture length, rupture width, and rupture area. Symbols are colored by event type: strike-slip faulting in red, reverse faulting in green, normal faulting in blue, and oblique faulting in orange. Data are plotted versus scaling relations from, respectively, top to bottom, Wells and Coppersmith (1994), Blaser et al. (2010), and Mai and Beroza (2000).

(slip) shown in Fig. 4. This observation is somewhat analogous to observations of discrepancies between on- and off-fault deformation during earthquakes (e.g., Gold et al., 2015), where geodetically measured on-fault co-seismic slip accounts for only ~72% of the total far-field displacement. Gold et al. (2015) also show that average surface slip is systematically lower than maximum slip, an observation that I show here holds for the entire ruptured fault.

This relationship makes no assumptions about the degree of and variability in geodetically measured coupling across fault surfaces. Rather, it implies that—to mirror the observed relationship between maximum potency and average potency—coupling must either be similarly (and somewhat predictably) spatially variable, or that co-seismic slip in large earthquakes does not release the entire accumulated strain budget on its fault segment. On average and over time, this relationship implies that a given fault segment does not release more than about 85% of its strain budget co-seismically in large earthquakes. In other words, average seismic coupling (i.e., the time-averaged ratio between strain accumulation and energy release) is either no more than about 0.85, or other processes (e.g., foreshocks, aftershocks, post-seismic slip, off-fault deformation) account for the remaining component of the budget (at least 15%). In reality, some combination of these factors is likely.

This relationship also has implications for earthquake cycles and repeatability. Given the implication discussed above that large earthquakes are unlikely to release the entire accumulated strain budget of a fault segment, it follows that the repeat time of that segment must be artificially advanced (the strain accumulation 'clock' does not start at zero). And, because maximum potency scales with and is larger than average potency, the region of maximum slip within a fault segment must move around between successive earthquakes on the segment—i.e., again, slip on

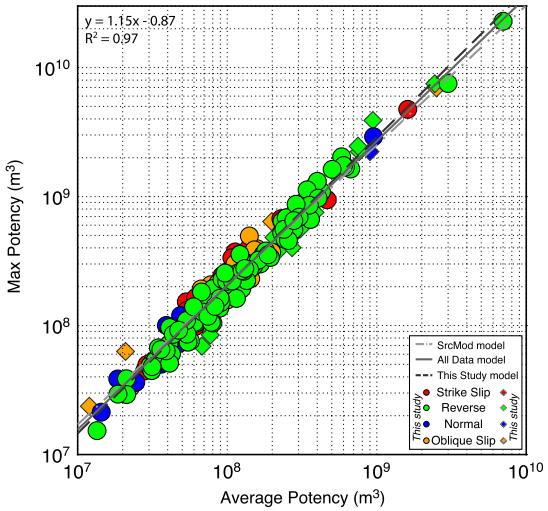

Fig. 4. Relationship between average potency and maximum potency, computed from earthquakes in this database (circles), and SRCMOD (diamonds). Symbols are colored by event type: strike-slip faulting in red, reverse faulting in green, normal faulting in blue, and oblique faulting in orange. The best-fitting linear relationship (for data from this database only) and associated R^2 value is displayed in the top left, and is plotted with a dashed black line. Best-fitting linear relationships for events from the SRCMOD database, and for all data, are plotted with a light gray dash-dot line, and a solid dark gray line, respectively.

the ruptured segment of a fault is not uniform. Thus, it may take several earthquake cycles for a fault segment to fully release its accumulated strain—perhaps giving the appearance of "earthquake super-cycles," as have been proposed in some subduction zone environments (e.g., Sieh et al., 2008).

5. Conclusions

I have presented a new and ever-expanding database of finite fault models created with a uniform modeling approach, and complete for all M 7.5+ shallow and intermediate depth earthquakes since 1990. The key advantage of this database is that it provides a comprehensive and consistent analysis of all large earthquakes. As such, models can be compared event-to-event without introducing significant uncertainties related to differing modeling approaches. The modeling approach adopted (Ji et al., 2002) is the same method used to study significant earthquakes at the USGS NEIC. As with other USGS event-based seismotectonic and impact related products, this ensures ease of access and the continuation of the database into the future.

As discussed, the database has a multitude of uses, from tsunami and hazard modeling to scaling relation computation. I have demonstrated how existing scaling relations compare to parameters of these models, and go on to show an intriguing relationship between maximum potency and average potency (and maximum potency and earthquake magnitude) that suggests average slip in an earthquake is linearly related to, but consistently and predictably less than, maximum slip. This relationship has important implications for maximum earthquake size for a given fault segment and earthquake repeat times, and thus associated estimates of seismic hazard.

Finally, as the global geophysics community looks towards the future of monitoring and research in subduction zones, this database can also be an important contribution to subduction zone observatories/initiatives worldwide.

Acknowledgements

Broadband seismic data from globally distributed seismometers available to the U.S. Geological Survey National Earthquake Information Center (NEIC) in real or near-real time (networks AD, AE, AF, AI, AK, AT, AU, AV, AZ, BE, BK, C, C1, CH, CI, CN, CT, CU, CX, CZ, DK, DR, EE, FN, G, GB, GE, GR, GS, GT, HE, HK, HU, IC, II, IM, IS, IU, IV, IW, JP, KC, KG, KN, KO, KR, KZ, LB, LD, LX, MB, MI, MN, MY, N4, NA, ND, NE, NM, OK, PE, PL, PR, PS, RM, RO, SK, SS, SV, TA, TM, TS, TU, TW, UO, US, UW, VE, WI and WM) and archived in the NEIC Central Waveform Buffer and at the Incorporated Research Institutions for Seismology Data Management Center were used in this study. Many of the figures were made using the Generic Mapping Tools software package (Wessel and Smith, 1991). I thank Chen Ji (University of California Santa Barbara) for his continued support of NEIC's finite fault modeling project, and Matthew Herman (Penn State University) for the deformation codes used for coulomb stress transfer calculations. Discussion with and reviews from Martin Mai, and an anonymous reviewer, helped to improve this manuscript.

Appendix A. Supplementary material

Supplementary material related to this article can be found online at http://dx.doi.org/10.1016/j.epsl.2017.04.003.

References

Alewine III, R.W., 1974. Application of Linear Inversion Theory Toward the Estimation of Seismic Source Parameters. Thesis. California Institute of Technology, Pasadena, California.

Allen, T.I., Hayes, G.P., 2017. Alternative rupture-scaling relationships for subduction interface and other offshore environments. Bull. Seismol. Soc. Am. 107 (3). http://dx.doi.org/10.1785/0120160255.

Ammon, C.J., Lay, T., Kanamori, H., Cleveland, M., 2011. A rupture model for the great 2011 Tohoku earthquake. Earth Planets Space 63, 33. http://dx.doi.org/10.5047/eps.2011.05.015.

Barnhart, W.D., Hayes, G.P., Samsonov, S.V., Fielding, E.J., Seidman, L.E., 2014a. Breaking the oceanic lithosphere of a subducting slab: the 2013 Khash, Iran earthquake. Geophys. Res. Lett. 41, 32–36. http://dx.doi.org/10.1002/2013GL058096.

Barnhart, W.D., Benz, H.M., Hayes, G.P., Rubinstein, J.L., Bergman, E., 2014b. Seismological and geodetic constraints on the 2011 Mw5.3 Trinidad, Colorado earthquake and induced deformation in the Raton Basin. J. Geophys. Res. 119, 7923–7933. http://dx.doi.org/10.1002/2014JB011227.

Blaser, L., Krüger, F., Ohrnberger, M., Scherbaum, F., 2010. Scaling relations of earthquake source parameter estimates with special focus on subduction environment. Bull. Seismol. Soc. Am. 100, 2914–2926.

Dahlen, F.A., Tromp, J., 1998. Theoretical Global Seismology. Princeton University Press, Princeton, NJ.

Fritz, H.M., Borrero, J.C., Synolakis, C.E., Okal, E.A., Weiss, R., Titov, V.V., Jaffe, B.E., Foteinis, S., Lynett, P.J., Chan, I.-C., Liu, P.L.-F., 2011. Insights on the 2009 South Pacific tsunami in Samoa and Tonga from field surveys and numerical simulations. Earth-Sci. Rev. 107, 66075.

Gold, R.D., Reitman, N.G., Briggs, R.W., Barnhart, W.D., Hayes, G.P., Wilson, E., 2015. On- and off-fault deformation associated with the September 2013 Mw 7.7 Balochistan earthquake: implications for geologic slip rate measurements. Tectonophysics 660, 65–78.

Hartzell, S.H., Helmberger, D.V., 1982. Strong-motion modeling of the Imperial Valley earthquake of 1979. Bull. Seismol. Soc. Am. 72 (2), 571–596.

Hartzell, S.H., Heaton, T.H., 1983. Inversion of strong ground motion and teleseismic waveform data for the fault rupture history of the 1979 Imperial Valley, California, earthquake. Bull. Seismol. Soc. Am. 73 (6), 1553–1583.

Hayes, G.P., 2011. Rapid source characterization of the 2011 Mw 9.0 off the Pacific coast of Tohoku earthquake. Earth Planets Space 63, 1–6.

Hayes, G.P., Earle, P.S., Benz, H.M., Wald, D.J., Briggs, R.W., the USGS/NEIC Earthquake Response Team, 2011. 88 hours: the U.S. Geological survey national earthquake information center response to the 11 March 2011 Mw 9.0 Tohoku earthquake. Seismol. Res. Lett. 82 (4), 481–493.

Hayes, G.P., Furlong, K.P., 2010. Quantifying potential tsunami hazard in the Puysegur subduction zone, south of New Zealand. Geophys. J. Int. 183 (3), 1512–1524.

Hayes, G.P., Wald, D.J., Johnson, R.L., 2012. Slab1.0: a three-dimensional model of global subduction zone geometries. J. Geophys. Res. 117, B01302. http://dx.doi.org/10.1029/2011JB008524.

Hayes, G.P., Bergman, E., Johnson, K., Benz, H.M., Brown, L., Meltzer, A., 2013. Seismotectonic framework of the February 27, 2010 Mw 8.8 Maule, Chile earthquake sequence. Geophys. J. Int. 195, 1034–1051. http://dx.doi.org/10.1093/gji/ggt238.

Hayes, G.P., Herman, M.W., Barnhart, W.D., Furlong, K.P., Riquelme, S., Benz, H.M., Bergman, E., Barrientos, S., Earle, P.S., Samsonov, S., 2014a. Continuing megathrust earthquake potential in Chile after the 2014 Iquique earthquake. Nature 512, 295–298. http://dx.doi.org/10.1038/nature13677.

Hayes, G.P., Furlong, K.P., Benz, H.M., Herman, H.W., 2014b. Triggered aseismic slip adjacent to the 6 February 2013 Mw8.0 Santa Cruz Islands megathrust earthquake. Earth Planet. Sci. Lett. 388, 265–272. http://dx.doi.org/10.1016/j.epsl.2013.11.010.

Hayes, G.P., Briggs, R.W., Barnhart, W.D., Yeck, W.L., McNamara, D.E., Wald, D.J., Nealy, J.L., Benz, H.M., Gold, R.D., Jaiswal, K.S., Marano, K., Earle, P.S., Hearne, M.G., Smoczyk, G.M., Wald, L.A., Samsonov, S., 2015. Rapid characterization of the 2015 Mw 7.8 Nepal (Gorkha) earthquake. Seismol. Res. Lett. 86 (6), 1557–1560. http://dx.doi.org/10.1785/0220150145.

Heaton, T.H., Helmberger, D.V., 1979. Generalized ray models of the San Fernando earthquake. Bull. Seismol. Soc. Am. 69 (5), 1311–1341.

Ide, S., 2007. Slip inversion. In: Kanamori, H. (Ed.), Earthquake Seismology. In: Treatise on Geophysics, vol. 4. Elsevier, Amsterdam, the Netherlands. ISBN 978-0-444-51932-0, pp. 193–224.

Ide, S., Baltay, A., Beroza, G.C., 2011. Shallow dynamic overshoot and energetic deep rupture in the 2011 Mw 9.0 Tohoku–Oki earthquake. Science 332 (6036), 1426–1429.

Ji, C., Wald, D.J., Helmberger, D.V., 2002. Source description of the 1999 Hector Mine, California, earthquake, part I: wavelet domain inversion theory and resolution analysis. Bull. Seismol. Soc. Am. 92, 1192–1207.

Ji, C., Helmberger, D.V., Wald, D.J., Ma, K.-F., 2003. Slip history and dynamic implications of the 1999 Chi–Chi, Taiwan, earthquake. J. Geophys. Res. 108. http://dx.doi.org/10.1029/2002JB001764.

Kikuchi, M., Kanamori, H., 1991. Inversion of complex body waves—III. Bull. Seismol. Soc. Am. 81 (6), 2335–2350.

Koketsu, K., Yokota, Y., Nishimura, N., Yagi, Y., Miyazaki, S.I., Satake, K., Furjii, Y., Miyake, H., Sakai, S., Yamanaka, Y., Okada, T., 2011. A unified source model for the 2011 Tohoku earthquake. Earth Planet. Sci. Lett. 310 (3), 480–487.

Langston, C.A., 1978. The February 9, 1971 San Fernando earthquake: a study of source finiteness in teleseismic body waves. Bull. Seismol. Soc. Am. 68, 1–29.

Lay, T., Ammon, C.J., Kanamori, H., Xue, L., Kim, M.J., 2011. Possible large near-trench slip during the 2011 Mw 9.0 off the Pacific coast of Tohoku Earthquake. Earth Planets Space 63 (7), 687–692.

Mai, P.M., Beroza, G.C., 2000. Source scaling properties from finite-fault-rupture models. Bull. Seismol. Soc. Am. 90 (3), 604–615.

Mai, P.M., Thingbaijam, K.K.S., 2014. SRCMOD: an online database of finite-fault rupture models. Seismol. Res. Lett. 85 (6), 1348–1357.

Mai, P.M., Shearer, P., Ampuero, J-P., Lay, T., 2016. Standards for documenting finite-fault earthquake rupture models. Seismol. Res. Lett. 87 (3), 712–718.

Mendoza, C., Hartzell, S.H., 1988. Aftershock patterns and main shock faulting. Bull. Seismol. Soc. Am. 78 (4), 1438–1449.

Newman, A.V., Hayes, G., Wei, Y., Convers, J., 2011. The 25 October 2010 Mentawai tsunami earthquake, from real-time discriminants, finite-fault rupture, and tsunami excitation. Geophys. Res. Lett. 38 (5). http://dx.doi.org/10.1029/2010GL046498.

Okada, Y., 1992. Internal deformation due to shear and tensile faults in a half-space. Bull. Seismol. Soc. Am. 82 (2), 1018–1040.

Okal, E.A., Fritz, H.M., Synolakis, C.E., Borrero, J.C., Weiss, R., Lynett, P.J., Titov, V.V., Foteinis, S., Jaffe, B.E., Liu, P.L.-F., Chan, I.-C., 2010. Field survey of the Samoa tsunami of 29 September 2009. Seismol. Res. Lett. 81 (4), 577–591.

Ozawa, S., Nishimura, T., Suito, H., Kobayashi, T., Tobita, M., Imakiire, T., 2011. Coseismic and postseismic slip of the 2011 magnitude-9 Tohoku–Oki earthquake. Nature 475 (7356), 373–376.

Petersen, M.D., et al., 2014. Documentation for the 2014 update of the United States national seismic hazard maps. US Geol. Survey Open-File Report 2014-1091. http://dx.doi.org/10.333/ofr20141091. 243 p.

Pollitz, F.F., Bürgmann, R., Banerjee, P., 2011. Geodetic slip model of the 2011 M9.0 Tohoku earthquake. Geophys. Res. Lett. 38 (7). http://dx.doi.org/10.1029/2011GL048632.

Riquelme, S., Fuentes, M., Hayes, G.P., Campos, J., 2015. A rapid estimation of near-field tsunami runup. J. Geophys. Res. 120 (9), 6487–6500.

Roeber, V., Yamazaki, Y., Cheung, K.F., 2010. Resonance and impact of the 2009 Samoa tsunami around Tutuila, American Samoa. Geophys. Res. Lett. 37 (21). http://dx.doi.org/10.1029/2010GL044419.

Sieh, K., Natawidjaja, D.H., Meltzner, A.J., Shen, C.-C., Cheng, H., Li, K.-S., Suwargadi, B.W., Galetzka, J., Philibosian, B., Edwards, R.L., 2008. Earthquake supercycles inferred from sea-level changes recorded in the corals of West Sumatra. Science 322 (5908), 1674–1678.

Shao, G., Li, X., Ji, C., Maeda, T., 2011. Focal mechanism and slip history of the 2011 Mw 9.1 off the Pacific coast of Tohoku Earthquake, constrained with teleseismic body and surface waves. Earth Planets Space 63 (7), 559–564.

Simons, M., Minson, S.E., Sladen, A., Ortega, F., Jiang, J., Owen, S.E., Meng, L., Ampuero, J.-P., Wei, S., Chu, R., Helmberger, D.V., Kanamori, H., Hetland, E., Moore, A.W., Webb, F.H., 2011. The 2011 magnitude 9.0 Tohoku-Oki earthquake: mosaicking the megathrust from seconds to centuries. Science 332 (6036), 1421–1425.

Skarlatoudis, A.A., Somerville, P.G., Thio, H.K., 2016. Source-scaling relations of interface subduction earthquakes for strong ground motion and tsunami simulation. Bull. Seismol. Soc. Am. 106 (4), 1652–1662.

Thingbaijam, K.K.S., Mai, P.M., 2016. Evidence for truncated exponential probability distribution of earthquake slip. Bull. Seismol. Soc. Am. 106 (4), 1802–1816.

Toda, S., Stein, R.S., Richards-Dinger, K., Bozkurt, S.B., 2005. Forecasting the evolution of seismicity in southern California: animations built on earthquake stress transfer. J. Geophys. Res. 110 (B5). http://dx.doi.org/10.1029/2004JB003415.

Toda, S., Lin, J., Stein, R.S., 2011. Using the 2011 Mw 9.0 off the Pacific coast of Tohoku Earthquake to test the Coulomb stress triggering hypothesis and to calculate faults brought closer to failure. Earth Planets Space 63 (7), 725–730.

Venkataraman, A., Kanamori, H., 2004. Observational constraints on the fracture energy of subduction zone earthquakes. J. Geophys. Res. 109, B05302. http://dx.doi.org/10.1029/2003JB002549.

Vigny, C., et al., 2011. The 2010 Mw 8.8 Maule megathrust earthquake of central Chile, monitored by GPS. Science 332 (6036), 1417–1421.

Wald, D.J., Worden, B.C., Lin, K., Pankow, K., 2005. ShakeMap Manual: Technical Manual, User's Guide, and Software Guide. U.S. Geological Survey, Techniques and Methods 12-A1. 132 pp.

Wald, D.J., Earle, P.S., Porter, K., Jaiswal, K., Allen, T.I., 2008. Development of the U.S. geological survey's prompt assessment of global earthquakes for response (PAGER) system. In: Proceedings of the 14th World Conf. on Earthq. Eng.. Beijing. 10 p.

Wang, et al., 2012. Real-time forecasting of the April 11, 2012 Sumatra tsunami. Geophys. Res. Lett. 39. http://dx.doi.org/10.1029/2012GL053081.

Wei, S., Graves, R., Helmberger, D., Avouac, J.P., Jiang, J., 2012. Sources of shaking and flooding during the Tohoku-Oki earthquake: a mixture of rupture styles. Earth Planet. Sci. Lett. 333, 91–100.

Wei, Y., Newman, A.V., Hayes, G.P., Titov, V.V., Tang, L., 2014. Tsunami forecast by joint inversion of real-time tsunami waveforms and seismic or GPS data: application to the Tohoku 2011 tsunami. Pure Appl. Geophys. 171 (12), 3281–3305.

Wells, D.L., Coppersmith, K.J., 1994. New empirical relationships among magnitude, rupture length, rupture width, rupture area, and surface displacement. Bull. Seismol. Soc. Am. 84, 974–1002.

Wessel, P., Smith, W., 1991. Free software helps map and display data. Eos Trans. AGU72, 441.

Yagi, Y., Fukahata, Y., 2011. Rupture process of the 2011 Tohoku–Oki earthquake and absolute elastic strain release. Geophys. Res. Lett. 38 (19). http://dx.doi.org/10.1029/2011GL048701.

Ye, L., Lay, T., Kanamori, H., Rivera, L., 2016. Rupture characteristics of major and great (Mw≥7.0) megathrust earthquakes from 1990 to 2015: 1. Source parameter scaling relationships. J. Geophys. Res. http://dx.doi.org/10.1002/2015JB012427.

Yue, H., Lay, T., 2011. Inversion of high-rate (1 sps) GPS data for rupture process of the 11 March 2011 Tohoku earthquake (Mw 9.1). Geophys. Res. Lett. 38 (7). http://dx.doi.org/10.1029/2011GL048700.